An Analysis of Unreliability and Asymmetry in Low-Power Wireless Links

Marco Zuniga and Bhaskar Krishnamachari

Abstract— **Experimental studies have demonstrated that the behavior of real links in low-power wireless networks (such as wireless sensor networks) deviates to a large extent from the ideal binary model used in several simulation studies. In particular, there is a large transitional region in wireless link quality that is characterized by significant levels of unreliability and asymmetry. Some works have shown that these unreliable and asymmetric links can significantly impact the performance of higher-layer protocols. In this paper, we provide a comprehensive analysis of the root causes of unreliability and asymmetry. In particular, we derive expressions for the distribution, expectation, and variance of the packet reception rate as a function of distance, and for the location and extent of the transitional region. These expressions incorporate important channel and radio parameters such as the path loss exponent and variance of the channel, and the modulation, encoding, and hardware variance of the radios.**

Index Terms— **Transitional region, log-normal path loss model, hardware variance, wireless sensor networks.**

I. Introduction

WIRELESS sensor network (WSN) protocols are often evaluated through simulations that make simplifying assumptions about the link layer, such as the ideal binary model. In this model, packets are received only within the circular radio range of the transmitter. However, the real characteristics of low-power wireless links differ greatly from those on the ideal model, chiefly among these differences are the unreliable and asymmetric nature of real links. The significant differences between the ideal model and the real behavior can lead to erroneous performance evaluation of upper-layer protocols (network layer and above).

Several studies ([1], [2], [3]) have classified low-power wireless links in three distinct reception regions: connected, transitional, and disconnected. In the connected region, links are often of good quality, stable and symmetric. On the other hand, the transitional region is characterized by the presence of unreliable and asymmetric links; and the disconnected region presents no practical links for transmission. Unfortunately, the transitional region is often quite significant in size, and in dense deployments such as those envisioned for sensor networks, a large number of the links in the network (even higher than 50% [2]) can be unreliable.

This work has been supported in part by NSF through grants numbered CANS-0325875, CANS-0347621, CANS-0435505, and CC-0430061. An earlier version of this paper appeared in the Proceedings of the IEEE SECON 2004, Santa Clara, CA, 2004.

M. Zuniga is with the Department of Electrical Engineering-Systems, University of Southern California, Los Angeles, CA 90089-0781 (e-mail: marcozun@usc.edu).

B. Krishnamachari is with the Department of Electrical Engineering-Systems, University of Southern California, Los Angeles, CA 90089-0781 (e-mail: bkrishna@usc.edu)

Recent studies have shown that unreliable and asymmetric links can have a major impact on the performance of upper-layer protocols. In [1], it is shown that the dynamics of even the simplest flooding mechanism can be significantly affected due to asymmetric and occasional long-distance links. In [6], it is argued that the routing structures formed taking into account unreliable links can be significantly different from the structures formed based on the simple binary model. Similarly, the authors of [7] report that such unreliable links can have a negative impact on routing protocols, particularly geographic forwarding schemes.

Other works ([3], [5]) have proposed mechanisms to take advantage of nodes in the transitional region. For instance, the authors of [5] found that protocols using the traditional minimum hop-count metric perform poorly in terms of throughput, and that a new metric called ETX (expected number of transmissions), which uses nodes in the transitional region, has a better performance.

The significant impact of real link characteristics on the performance of upper-layer protocols has created an increased understanding of the need for realistic link layer models for wireless sensor networks. In order to address this need, some recent works ([3], [7], [8]) have proposed new link models based on empirical data. However, these models do not provide significant mathematical insight into how the channel and radio dynamics affect link unreliability and asymmetry. Also, some of these works ([19], [3]) are valid only for the specific channel and radio parameters used in the deployment.

In this study, we use analytical tools from communication theory, simulations and experiments to present an in-depth analysis of unreliable and asymmetric links in low-power multi-hop wireless networks. The main contributions of this work are twofold. First, it allows us to quantify the impact of the wireless environment and radio characteristics on link reliability and asymmetry. And second, we propose a systematic way to generalize models for the link layer that can be used to enhance simulation accuracy.

We also derive expressions for the packet reception rate as a function of distance, and for the size of the transitional region. These expressions incorporate several radio parameters such as modulation, encoding, output power, frame size, receiver noise floor and hardware variance; as well as important channel parameters, namely, the path loss exponent and the log-normal variance.

Table I presents the organization of the paper. In section II, we present the related work. Section III studies the impact of multi-path on link reliability. First, we present a model for the packet reception rate as a function of distance in subsection III-

Topic	Section
Related Work	II
Channel Dynamics	III
Link Model	III-A
Impact on Link Reliability	III-B
Expectation and Variance of PRR	III-C
Comparison with Available Models	III-D
Hardware Variance	IV
Hardware Variance Model	IV-A
Impact on Link Asymmetry	IV-B
Impact on Link Reliability	IV-C
Empirical Validation	V

TABLE I
ORGANIZATION

A. Based on this model, in subsection III-B we study the impact of channel and radio parameters on link reliability by analyzing their effect on the extent of the transitional region. Then, in subsection III-C we present approximate expressions for the expectation and variance of the packet reception rate as a function of distance. The section ends with a comparison of available link models with the one proposed in this work (subsection III-D).

We study the impact of hardware variance in section IV. Hardware variance has already been identified as the cause of link asymmetry [8], in addition, we also show that it can play a significant role on the extent of the transitional region. In subsection IV-A, we present a model for hardware variance. Based on this model, the impact of hardware variance on link asymmetry and reliability is quantified in subsections IV-B and IV-C, respectively. Finally, in section V we present empirical measurements based on a test-bed of mica2 motes which validate some analytical insights of our work. Our conclusions are presented in section VI.

Before proceeding we present the scope of our work. Our study is focused on static and low-dynamic environments and it does not consider interference effects nor the non-isotropic property of radio coverage. However, our work can be complemented with other research efforts to incorporate these dynamics. For instance, in [13] the authors focus on the study of interference in wireless sensor networks, Cerpa *et. al.* [19] study some temporal properties and [7] provides an interesting model for the non-isotropic characteristic of radio coverage, the models presented in these works can be used to complement ours. Appendix I presents some guidelines on how to combine the non-isotropic RIM model [7] with our work.

II. Related Work

The unrealistic nature of some common assumptions used in mobile ad-hoc networks (MANET) research is presented in [6]. In real scenarios, packet losses lead to different connectivity graphs, and coverage ranges that are neither circular nor convex and are often noncontiguous.

Several researchers have pointed out that simplistic assumptions may lead to erroneous performance evaluations of upper-layer protocols. In one of the earliest works [1], Ganesan *et al.* present empirical results on the behavior of a simple flooding in a dense sensor network. They found that the flooding tree exhibits a high clustering behavior, in contrast to the more uniformly distributed tree obtained with the ideal binary model.

In [5], De Couto *et al.* present measurements for DSDV and DSR over a 29 node 802.11b test-bed and show that when the real channel characteristics are not taken into account, the minimum hop-count metric has poor performance. By incorporating the effects of link loss ratios, asymmetry, and interference, they present the expected transmission count metric which finds high throughput paths. Along similar lines, Woo *et al.* [3] study the effect of link connectivity on distance-vector based routing in sensor networks. By evaluating link estimator, neighborhood table management, and reliable routing protocols techniques, they found that cost-based routing using a minimum expected transmission metric shows good performance.

Zhou *et al.* [7] reported that radio irregularity has a significant impact on routing protocols, but a relatively small impact on MAC protocols. They found that location-based routing protocols, such as geographic routing perform worse in the presence of radio irregularity than on-demand protocols, such as AODV and DSR.

Through empirical studies the previous works bring to light the impact that unreliable and asymmetric links have on protocol performance at different layers. Nevertheless, while an on-site deployment is arguably the best testing procedure for small-scale networks, it may be unfeasible for medium and large-scale networks, for which simulators are usually the best option. In order to help overcome this problem some tools and models have been recently proposed to obtain more accurate link-layer models.

In [3], the authors derive a packet loss model based on aggregate statistical measures such as mean and standard deviation of packet reception rate. The model assumes a Gaussian distribution of the packet reception rate for a given transmitter-receiver distance which, as it will be shown in Section III, is not accurate.

Using the SCALE tool [4], Cerpa *et al.* [8] identify other factors for link modeling. They capture features of groups of links associated with a particular receiver, a particular transmitter, and links associated with a group of radios in close proximity. Using several statistical techniques they provide a spectrum of models of increasing complexity and increasing accuracy.

A more recent model, called the Radio Irregularity Model (RIM), was proposed in [7]. Based on experimental data, RIM provides a radio model that takes into account both the non-isotropic properties of the propagation media and the heterogeneous properties of devices to build a richer link model.

Temporal properties in dynamic environments have been studied as well. In [19], the authors study short term temporal issues such as autocorrelation of individual and reverse links,

Description	Symbol
Packet Reception Rate Parameters	
- packet reception rate (PRR)	Ψ
- a specific PRR value in the range of Ψ	ψ
- high PRR	ψ_h
- low PRR	ψ_ℓ
Signal to Noise Ratio Parameters	
- signal to noise ratio (SNR)	Υ
- a specific SNR value in the range of Υ	γ
- SNR value corresponding to ψ_h	γ_h
- SNR value corresponding to ψ_ℓ	γ_ℓ
- mean of SNR (Gaussian) for distance d	$\mu(d)$
- bit error rate as a function of SNR	β
- bit error rate as a function of SNR in dB	$\mathcal{B}$
Channel Parameters	
- path loss exponent	η
- standard deviation	σ
- output power	P_t
- received power	P_r
- noise floor	P_n
- Gaussian random variable	$\mathcal{N}$
Transitional Region Parameters	
- transitional region coefficient	Γ
- beginning of transitional region	d_b
- end of transitional region	d_e

TABLE II
MATHEMATICAL NOTATION

and long term temporal properties such as the length of time the channel needs to be measured and how often to obtain accurate link quality metrics. The authors also propose new routing algorithms to take advantage of the temporal properties of wireless links.

While the described models are important steps toward a realistic link quality model, they do not provide significant mathematical insight on how the channel and radio parameters affect link unreliability and asymmetry. Also, some of these models ([3], [8]) do not provide a systematic way to generalize the models (i.e., extend their validity and accuracy) beyond the specific radio and environment conditions of the experiments from which the models are derived.

On the other hand, years of research in wireless communications, particularly cellular networks, provide a rich set of models and tools for analyzing the physical layer [23][1]. Two of these tools are of significant importance to understand the transitional region, the log-normal path loss model (to model the wireless channel) and the bit-error performance of various modulation and encoding schemes with respect to the signal to noise ratio (to model the radio).

Hitherto, the research done has identified the link-layer modeling problem and its impact on upper-layer protocols, it also has identified some of its causes and proposed some realistic link quality models. However, what is missing is a clear analytical understanding of the root causes of the link behavior. Our work presents an in-depth analysis on unreliable and asymmetric links and provides simple analytical models for the link layer.

[1]In cellular systems the transitional region is not of interest (except for modeling inter-cell interference) as cells are designed to fit only the connected region.

III. IMPACT OF CHANNEL DYNAMICS

The extent of the transitional region is the result of placing specific devices, for example mica2 motes, in an specific environment, like the aisle of a building. If the characteristics of one of these elements is altered (radio or channel) then the extent of the transitional region is also altered. With the intent of analyzing how the channel and the radio determine this extent; first, we define models for both elements, and subsequently study their interaction. Then, we present approximated expressions for the expectation and variance of the packet reception rate with respect to distance. Finally, we compare our model with a previously proposed model.

From the network-layer perspective, a desired abstraction for link quality is the packet reception rate as a function of distance. This abstraction can be derived by composing the channel model, which provides the received signal strength (RSS) as a function of distance, with the radio-receiver model, which provides the packet reception rate (PRR) as a function of the signal to noise ratio (SNR).

In the remainder of the paper, the SNR function is denoted by Υ and the PRR function by Ψ. Also, the lowercase greek letters: $\gamma = \Upsilon(.)$ and $\psi = \Psi(.)$, represent values taken by Υ and Ψ for specific points in their respective domains. Table II presents a summary of the notation used in this paper.

A. Channel and Radio Receiver Models

Channel: When an electromagnetic signal propagates, it may be diffracted, reflected and scattered. These effects have two important consequences on the signal strength. First, the signal strength decays exponentially with respect to distance. And second, for a given distance d, the signal strength is random and log-normally distributed about the mean distance dependent value.

Due to the unique characteristics of each environment, most radio propagation models use a combination of analytical and empirical methods. One of the most common radio propagation models is the log-normal path loss model [23]. This model can be used for large and small coverage systems [11]. Furthermore, empirical studies have shown that the log-normal model provides more accurate multi-path channel models than Nakagami and Rayleigh for indoor environments [12].

According to this model the received power (P_r) in dB is given by:

$$P_r(d) = P_t - PL(d_0) - 10\ \eta\ log_{10}(\frac{d}{d_0}) + \mathcal{N}(0,\sigma) \quad (1)$$

Where P_t is the output power, η is the path loss exponent that captures the rate at which signal decays with respect to distance, $\mathcal{N}(0,\sigma)$ is a Gaussian random variable with mean 0 and variance σ (standard deviation due to multi-path effects), and $PL(d_0)$ is the power decay for the reference distance d_0.

Equation 1 does not consider non-isotropic transmission, which is an important characteristic of low-power wireless links. In Appendix I we present some guidelines on how to incorporate these non-isotropic effects in our model by using the expressions derived in the RIM model [7]. Appendix I

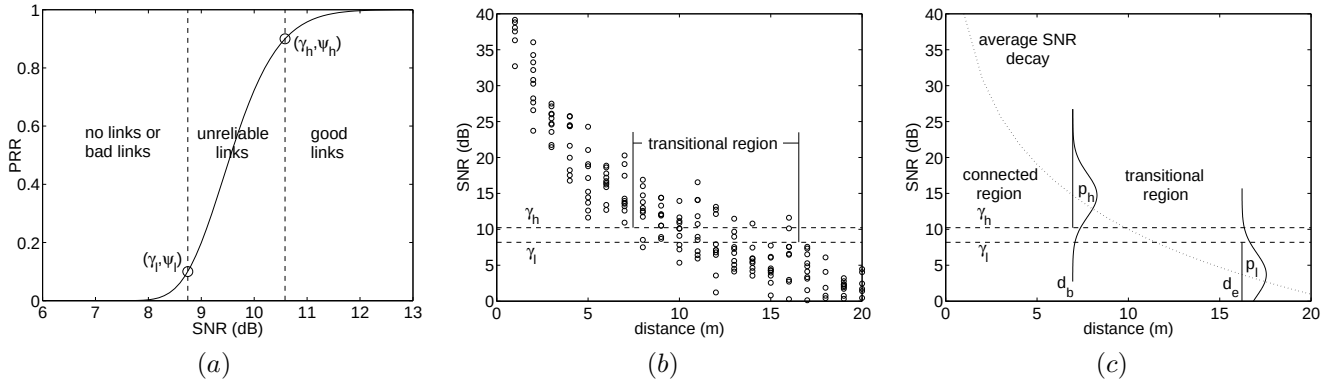

Fig. 1. (a) A receiver response where ψ_ℓ and ψ_h determine different regions of link quality, (b) Interaction of γ_ℓ and γ_h with the channel to determine the transitional region, (c) Analytical representation of equations 6 and 7.

also presents some information on how to include the path-loss effect caused by obstacles.

Radio Receiver: The receiver response is given by the packet reception rate as a function of the SNR. The packet reception rate can be derived from bit-error-rates expressions that are widely available in the wireless communication literature.

For a modulation M, the packet reception rate (Ψ) is defined in terms of the bit-error-rate (β_M) as [2]:

$$\Psi(\gamma) = (1 - \beta_M(\gamma))^f \tag{2}$$

Where f is the number of bits transmitted, and step 3 in Table VII presents expressions of β_M for some common narrowband modulation schemes.

β_M is a function of the SNR. The SNR can be obtained from equation 1 and is given by:

$$\begin{aligned} \Upsilon(d) &= P_r(d) - P_n \\ &= \mathcal{N}(\mu(d), \sigma) \end{aligned} \tag{3}$$

Where $\mathcal{N}(\mu(d), \sigma)$ is a Gaussian random variable with mean $\mu(d)$, variance σ^2 and P_n is the noise floor[3]. $\mu(d)$ can be derived by inserting equation 1 in equation 3, which leads to:

$$\mu(d) = P_t - PL(d_0) - 10\ \eta\ log_{10}(\frac{d}{d_0}) - P_n \tag{4}$$

Given that the SNR in equation 3 is in dB, let us redefine the packet reception rate in equation 2 as a function of the SNR in dB. Denoting $\omega(x) = 10^{x/10}$ and the bit-error-rate for SNR in dB as $\mathcal{B}_M(\gamma_{dB}) = \beta_M(\omega\ (\gamma_{dB}))$, the packet reception rate Ψ can be redefined as:

$$\Psi(\gamma_{dB}) = (1 - \mathcal{B}_M(\gamma_{dB}))^f \tag{5}$$

[2]For ease of explanation, the encoding is assumed to be NRZ. Table VII presents expressions for other encoding techniques.

[3]The focus of this paper is on static interference-free environments. In these scenarios P_n is given only by thermal noise and is constant, which in turn leads to constant packet reception rates in time as shown in [15]. Nevertheless, in most scenarios P_n changes with time either because of interference or because of large changes in temperature. For these scenarios P_n can be modeled as a random processes.

While the previous equation is general and valid for any modulation M, the figures in this section assume Non-Coherent FSK (NCFSK) modulation. The figures are for illustrative purposes and any modulation would serve that purpose. NCFSK was chosen because the empirical evaluation presented in section V uses NCFSK radios (the CC1000 equipped mica2 motes).

B. Impact on Link Reliability (Extent of Transitional Region)

In this subsection our aim is to quantify the impact of channel dynamics on the extent of the transitional region. Given that the channel model is a function of the SNR vs distance and the receiver response is a function of the PRR vs SNR, we can derive the behavior of the PRR vs distance by linking both expressions through the SNR metric. First, we derive the SNR values that determine the beginning and end of the transitional region in the receiver response, and then we determine how this SNR values map to distance in the channel model.

Even though there are no strict definitions for the different regions in the literature, one valid definition is the following:

Definition 1: In the connected region links have a high probability ($> p_h$) of having high packet reception rates ($> \psi_h$).

Definition 2: In the disconnected region links have a high probability ($> p_\ell$) of having low packet reception rates ($< \psi_\ell$).

Where p_h and p_ℓ can be chosen as any numbers close to 1 and 0 respectively.

Letting $\mathcal{B}_M^{-1}(.)$ be the inverse[4] of $\mathcal{B}_M(\gamma_{dB})$, and $\Psi^{-1}(\psi) = \mathcal{B}_M^{-1}(1 - \psi^{1/f})$ the inverse of Ψ; the PRR values ψ_h and ψ_ℓ, from the definitions above, can be mapped to their corresponding SNR values in dB: $\gamma_h = \Psi^{-1}(\psi_h)$ and $\gamma_\ell = \Psi^{-1}(\psi_\ell)$. These SNR values determine the beginning and end of the transitional region.

[4]BER functions are injective, hence, while there might not be a closed-form expression for their inverse function, the SNR in the domain can always be obtained numerically.

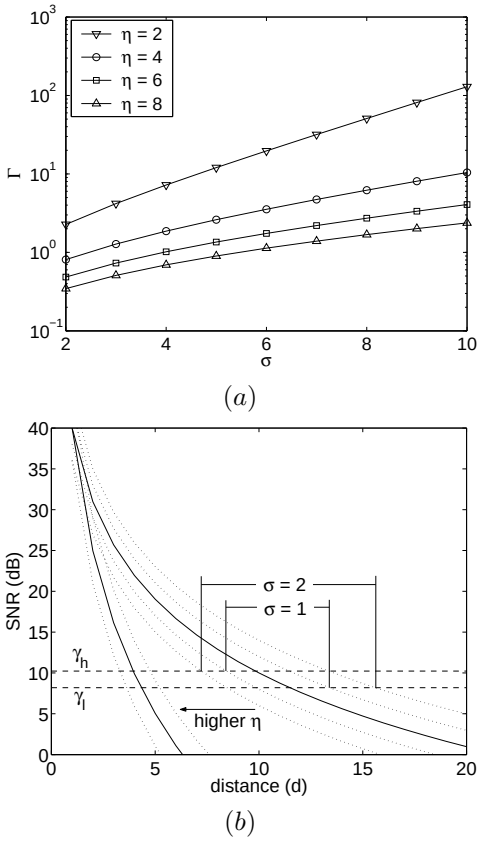

Fig. 2. Impact of σ and η on extent of transitional region. (a) Γ for different values of η and σ, (b) solid curves represent average power decay, and dotted lines the [-2σ, 2σ] interval of the variance.

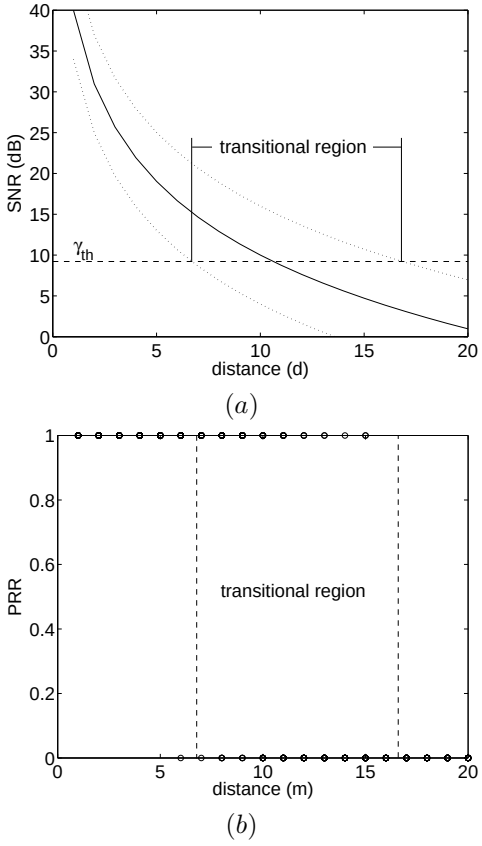

Fig. 3. Impact of perfect receiver threshold on extent of transitional region, (a) Analytical representation, (b) An instance of PRR vs distance.

Figure 1 (a) shows how ψ_h and ψ_ℓ determine three different regions in the radio-receiver response (equation 5), and Figure 1 (b) shows how γ_h and γ_ℓ interact with the channel (equation 3) to determine the extent of the connected, transitional and disconnected regions.

According to Definition 1 the beginning of the transitional region (d_b) satisfy the following condition:

$$\begin{array}{lll} & p(\Psi > \psi_h) & = p_h, \quad \because \Psi \text{ is injective} \\ \Rightarrow & p(\Upsilon > \gamma_h) & = p_h, \quad \because \Upsilon \text{ is Gaussian} \\ \Rightarrow & Q(\frac{\gamma_h - \mu(d_b)}{\sigma}) & = p_h \end{array} \tag{6}$$

And according to Definition 2 the end of transitional region (d_e) satifies:

$$\begin{array}{lll} & p(\Psi < \psi_\ell) & = p_\ell, \quad \because \Psi \text{ is injective} \\ \Rightarrow & p(\Upsilon < \gamma_\ell) & = p_\ell, \\ \Rightarrow & p(\Upsilon \geq \gamma_\ell) & = (1 - p_\ell), \quad \because \Upsilon \text{ is Gaussian} \\ \Rightarrow & Q(\frac{\gamma_\ell - \mu(d_e)}{\sigma}) & = (1 - p_\ell) \end{array} \tag{7}$$

Where $Q(.)$ is the tail integral of a unit Gaussian probability density function (*pdf*) and $\mu(.)$ is given by equation 4. Figure 1 (c) depicts an analytical representation of the previous equations. This figure shows how the interaction between the channel and the receiver response determine the extent of the transitional region. Finally, d_b and d_e can be derived from equations 6 and 7:

$$\begin{array}{l} d_b = 10^{\frac{\gamma_h - \sigma Q^{-1}(p_h) - P_t + P_n + PL(d_0)}{-10n}} \\ d_e = 10^{\frac{\gamma_\ell - \sigma Q^{-1}(1-p_\ell) - P_t + P_n + PL(d_0)}{-10n}} \end{array} \tag{8}$$

While equation 8 provides absolute values for the extent of the different regions, it may not be useful to compare the link-quality of different scenarios. With that aim, we define the *transitional region coefficient* Γ which is the ratio of the extent of the transitional with respect to the extent of the connected region.

$$\begin{array}{ll} \Gamma & = \frac{d_e - d_b}{d_b} \\ & = 10^{\frac{(\gamma_h - \gamma_\ell) + \sigma(Q^{-1}(1-p_\ell) - Q^{-1}(p_h))}{10n}} - 1 \end{array} \tag{9}$$

The lower the coefficient Γ the smaller the transitional region compared to the connected one. For example, for the ideal binary model, where $\gamma_h = \gamma_\ell$ and $\sigma = 0$, the coefficient $\Gamma = 0$. Notice that Γ is independent of the noise floor P_n and output power P_t; a higher output power would increase the connected region, but it would increase the transitional region as well, keeping a constant ratio.

Equation 9 predicts the impact of the channel on the transitional region. Given that p_h and p_ℓ are high probabilities, $(Q^{-1}(1-p_\ell) - Q^{-1}(p_h))$ is positive, and hence, while a small σ decreases the relative extent of the transitional region, a small η increases it. Therefore, scenarios with high η and low σ reduce the relative size of the transitional region.

Figure 2 (a) presents Γ for different values of η and σ, where $p_\ell = p_h = 0.9$, $\gamma_h = 10.23$ dB and $\gamma_\ell = 8.20$ dB [5].

Figure 2 (b) depicts analytically the impact of η and σ on the extent of the transitional region. The SNR bounds on the radio receiver (γ_h and γ_ℓ) are fixed and independent of the environment. When σ increases from 1 to 2 the signal values (y-axis) have a higher probability of entering the transitional region at closer distances from the transmitter and leaving it at farther distances, which results in a larger transitional region. When η is increased (left arrow), the faster decay of the signal strength decreases the width of the transitional region.

Equation 9 also predicts the impact of the receiver. The sharper the receiver threshold, the smaller $(\gamma_h - \gamma_\ell)$ and the smaller the Γ coefficient. However, even with a perfect threshold receiver ($\gamma_h = \gamma_\ell$), as the one used on the ideal model, the transitional region would still exist due to channel dynamics (σ). Figure 3 (a) depicts analytically the behavior of a perfect threshold receiver in a real channel, and Figure 3 (b) shows an instance of the link behavior. Notice that in this hypothetical scenario the transitional region would consist only of 0/1 links.

The model also allows to provide the cumulative distribution function (*cdf*) of the packet reception rate as a function of distance. According to equation 5:

$$\begin{aligned} F(\psi) &= p(\Psi < \psi) \\ &= p(\Upsilon < \Psi^{-1}(\psi)) \\ &= 1 - Q(\tfrac{\Psi^{-1}(\psi) - \mu(d)}{\sigma}) \end{aligned} \tag{10}$$

Where $\mu(d)$ is the average SNR decay (equation 4). Figure 4 shows an example of the cumulative distribution $F(\psi)$ for $\eta = 3$ and $\sigma = 3$. Three different transmitter-receiver distances are shown: end of connected region, middle of transitional and beginning of disconnected region. We can notice that independent of the region where the receiver is, the link has a higher probability of being either good or bad (above 0.9 or below 0.1 PRR) than being unreliable (between 0.9 and 0.1). For instance, in the middle of the transitional region the link has a 30% probability of being unreliable; and the probability of observing unreliable links at the end of the connected region or at the beginning of the disconnected region is small ($< 5\%$). Empirical measurements in [8], [14] agree with the analytical *cdf* in equation 10.

It is important to remark that the obtained *cdf*s are valid only for the scope of this work (static and low-dynamic environments); highly dynamic environments add a new dimension of time to the *cdf*s.

C. Expectation and Variance of Packet Reception Rate

Even though a longer distance does not necessarily imply a lower packet reception rate, the expected value of the packet reception rate does decrease monotonically with distance in a given propagation direction[6]. In this subsection, we present approximate expressions for the expectation and variance of the packet reception rate Ψ. These expressions are important because they confirm mathematically that the transitional region has a higher variability in PRR than the connected region.

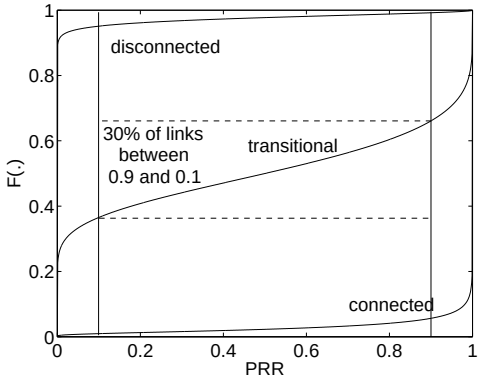

Fig. 4. *cdf*s for packet reception rate for receivers in different regions in a specific environment ($\eta = 3$, $\sigma = 3$).

First we present the general expressions for the expectation and variance in equations 11 and 12 . These expression depend on the PRR versus distance function (receiver response given in equation 5) and the probability density function (*pdf*) of the SNR for a given distance d (which is log-normally distributed). Given the mathematical complexity of dealing with the receiver response and the *pdf*, we present linear approximations for both, which are used to derive approximate expressions for the expectation and variance of the packet reception rate Ψ.

In general, the first two moments of Ψ are defined by:

$$E[\Psi] = \int_{-\infty}^{\infty} \Psi(\gamma_{dB}) f(\gamma_{dB}, d)\ \delta\gamma_{dB} \tag{11}$$

$$E[\Psi^2] = \int_{-\infty}^{\infty} \Psi^2(\gamma_{dB}) f(\gamma_{dB}, d)\ \delta\gamma_{dB} \tag{12}$$

Where $f(\gamma_{dB}, d)$ represents the *pdf* of SNR (a Gaussian random variable with parameters $\mu(d)$ and σ).

The sharp thresholds of Ψ and Ψ^2 permit linear approximations:

$$\Psi(\gamma) \approx \Psi_L(\gamma) = \begin{cases} 0, & \gamma \le \gamma_{0e} \\ m_e\ \gamma + b_e, & \gamma_{0e} < \gamma < \gamma_{1e} \\ 1, & \gamma \ge \gamma_{1e} \end{cases} \tag{13}$$

$$\Psi^2(\gamma) \approx \Psi_L^2(\gamma) = \begin{cases} 0, & \gamma \le \gamma_{0v} \\ m_v\ \gamma + b_v, & \gamma_{0v} < \gamma < \gamma_{1v} \\ 1, & \gamma \ge \gamma_{1v} \end{cases} \tag{14}$$

Where m_e, m_v and b_e, b_v are the slopes and y-intercepts of the linear approximations Ψ_L and Ψ_L^2, and γ is in dB.

[5] γ_h and γ_ℓ were obtained for a NCFSK radio with Manchester encoding and a frame size of 100 bytes. Different modulations, encoding and packet sizes do not have a significant impact on Γ, and the results are not presented due to space constraints. Some of these results are available in [14].

[6] The radio model used in this work is isotropic, but this is not true of practical antennas. By linearity of expectation, since $E[\Psi_a(d)]$ is monotonic with distance for a given propagation direction a, it can be shown that the expected PRR averaged over all angles is also monotonic with distance; however, it should be kept in mind that expected PRR values at different angles may show non-distance-monotonic behavior with respect to each other.

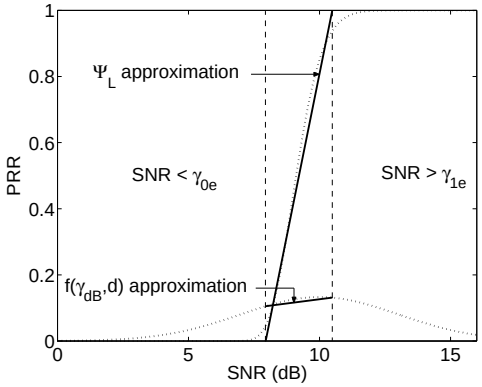

Fig. 5. Linear approximation of receiver threshold and Gaussian SNR, the mean of the Gaussian depends on the transmitter-receiver distance

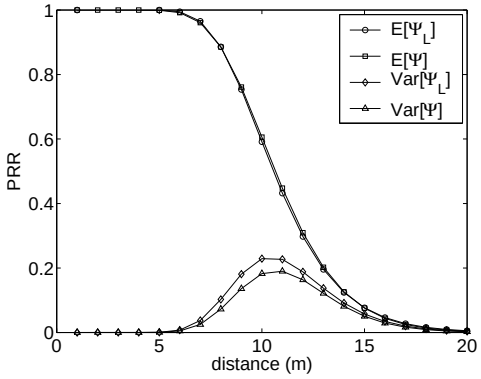

Fig. 6. Comparison of E[Ψ] and Var[Ψ] with their linear approximations, E[Ψ_L] and Var[Ψ_L].

Figure 5 (a) shows the approximation procedure for Ψ_L; the procedure for Ψ_L^2 is similar. The mechanism to obtain the slopes, y-intercepts and limit points of equations 13 and 14 is presented later.

The linear models lead to the following approximations of equations 11 and 12:

$$\begin{aligned} E[\Psi] &\approx \int_{\gamma_{0e}}^{\infty} \Psi_L(\gamma_{dB})\ f(\gamma_{dB},d)\ \delta\gamma_{dB} \\ &= \int_{\gamma_{0e}}^{\gamma_{1e}} (m_e\ \gamma + b_e)\ f(\gamma_{dB},d)\ \delta\gamma_{dB} \\ &\quad + Q(\tfrac{\gamma_{1e}-\mu(d)}{\sigma}) \end{aligned} \tag{15}$$

$$\begin{aligned} E[\Psi^2] &\approx \int_{\gamma_{0v}}^{\infty} \Psi_L^2(\gamma_{dB})\ f(\gamma_{dB},d)\ \delta\gamma_{dB} \\ &= \int_{\gamma_{0v}}^{\gamma_{1v}} (m_v\ \gamma + b_v)\ f(\gamma_{dB},d)\ \delta\gamma_{dB} \\ &\quad + Q(\tfrac{\gamma_{1v}-\mu(d)}{\sigma}) \end{aligned} \tag{16}$$

In the above approximations $f(\gamma_{dB},d)$ is evaluated separately on intervals $[\gamma_{0e},\gamma_{1e}]$ and $[\gamma_{0v},\gamma_{1v}]$ for $E[\Psi]$ and $E[\Psi^2]$, respectively. Both intervals represent the linear approximations of the sharp thresholds of Ψ and Ψ^2, and these thresholds are narrow compared to the $[\mu-4\sigma,\ \mu+4\sigma]$ domain of $f(\gamma_{dB},d)$[7], hence, linear approximations can be used as well for $f(\gamma_{dB},d)$ in $[\gamma_{0e},\gamma_{1e}]$ and $[\gamma_{0v},\gamma_{1v}]$.

Let us denote $f_{\Psi}(\gamma_{dB},d)$ and $f_{\Psi^2}(\gamma_{dB},d)$ as the linear approximations of $f(\gamma_{dB},d)$ for intervals $[\gamma_{0e},\gamma_{1e}]$ and $[\gamma_{0v},\gamma_{1v}]$:

$$f_{\Psi}(\gamma_{dB},d) = m_{ge}\gamma + b_{ge} \tag{17}$$

$$f_{\Psi^2}(\gamma_{dB},d) = m_{gv}\gamma + b_{gv} \tag{18}$$

where:

$$\begin{array}{ll} m_{ge} = \frac{f(\gamma_{1e},d)-f(\gamma_{0e},d)}{\gamma_{1e}-\gamma_{0e}} & b_{ge} = \frac{f(\gamma_{0e},d)\gamma_{1e}-f(\gamma_{1e},d)\gamma_{0e}}{\gamma_{1e}-\gamma_{0e}} \\ m_{gv} = \frac{f(\gamma_{1v},d)-f(\gamma_{0v},d)}{\gamma_{1v}-\gamma_{0v}} & b_{gv} = \frac{f(\gamma_{0v},d)\gamma_{1v}-f(\gamma_{1v},d)\gamma_{0v}}{\gamma_{1v}-\gamma_{0v}} \end{array}$$

Figure 5 shows the approximation procedure for $f_{\Psi}(\gamma_{dB},d)$ (Gaussian SNR curve for $E[\Psi]$); the procedure for $f_{\Psi^2}(\gamma_{dB},d)$ is similar.

[7]While the domain of a Gaussian random variable is $[-\infty,+\infty]$, the interval $[\mu-4\sigma,\mu+4\sigma]$ contains most of the probability space (.999), and it is wide compared to the sharp threshold of the receiver for common values of σ ([10]).

Finally, based on equations 15 and 16, the first and second moment approximations of the packet reception rate are given by:

$$\begin{aligned} E[\Psi] &\approx \int_{\gamma_{0e}}^{\gamma_{1e}} (m_e\ \gamma + b_e)\ f_{\Psi}(\gamma_{dB},d)\ \delta\gamma_{dB} \\ &\quad + Q(\tfrac{\gamma_{1e}-\mu(d)}{\sigma}) \\ &= \int_{\gamma_{0e}}^{\gamma_{1e}} (m_e\ \gamma + b_e)\ (m_{ge}\ \gamma + b_{ge})\ \delta\gamma_{dB} \\ &\quad + Q(\tfrac{\gamma_{1e}-\mu(d)}{\sigma}) \\ &= ((m_e + m_{ge})\tfrac{\gamma^3}{3} + (b_e m_{ge} + b_{ge} m_e)\tfrac{\gamma^2}{2} \\ &\quad + b_e b_{ge}\gamma)|_{\gamma_{0e}}^{\gamma_{1e}} + Q(\tfrac{\gamma_{1e}-\mu(d)}{\sigma}) \end{aligned} \tag{19}$$

$$\begin{aligned} E[\Psi^2] &\approx \int_{\gamma_{0v}}^{\gamma_{1v}} (m_v\ \gamma + b_v)\ f_{\Psi^2}(\gamma_{dB},d)\ \delta\gamma_{dB} \\ &\quad + Q(\tfrac{\gamma_{1v}-\mu(d)}{\sigma}) \\ &= \int_{\gamma_{0v}}^{\gamma_{1v}} (m_v\ \gamma + b_v)\ (m_{gv}\ \gamma + b_{gv})\ \delta\gamma_{dB} \\ &\quad + Q(\tfrac{\gamma_{1v}-\mu(d)}{\sigma}) \\ &= ((m_v + m_{gv})\tfrac{\gamma^3}{3} + (b_v m_{gv} + b_{gv} m_v)\tfrac{\gamma^2}{2} \\ &\quad + b_v b_{gv}\gamma)|_{\gamma_{0v}}^{\gamma_{1v}} + Q(\tfrac{\gamma_{1v}-\mu(d)}{\sigma}) \end{aligned} \tag{20}$$

In general, the parameters of Ψ_L and Ψ_L^2 (slopes, y-intercepts and limit points of equations 13 and 14) can be obtained by curve-fitting Ψ and Ψ^2 through least squares regression techniques, nevertheless, our studies suggest that choosing a line that passes through points A and B with PRRs of 0.1 and 0.9 provides an accurate approximation[8]. Hence, A and B defined as (Ψ^{-1}(0.1), 0.1) and (Ψ^{-1}(0.9), 0.9) can be used to obtain the different parameters of Ψ_L:

$$\begin{array}{ll} m_e = \frac{0.9-0.1}{\gamma_B-\gamma_A} & b_e = \frac{0.1\gamma_B-0.9\gamma_A}{\gamma_B-\gamma_A} \\ \gamma_{0v} = \frac{-b_e}{m_e} & \gamma_{1v} = \frac{1-b_e}{m_e} \end{array}$$

Where $\gamma_A = \Psi^{-1}(0.1)$ and $\gamma_B = \Psi^{-1}(0.9)$, both in dB. For Ψ_L^2, points A and B are ($\Psi^{-1}(\sqrt{0.1})$, 0.1) and ($\Psi^{-1}(\sqrt{0.9})$, 0.9).

Figure 6 shows an example of numerically calculated curves for the expectation and variance (from equations 11 and 12), and their approximations through equations 19 and 20 for $\eta = 3$ and $\sigma = 3$. In general, the error depends on the parameters of $f(\gamma_{dB},d)$ (*pdf* of SNR). The smaller σ, the

[8]Actually, no significant differences were found if points A and B are chosen in intervals [0.01, 0.2] and [0.8, 0.99], respectively.

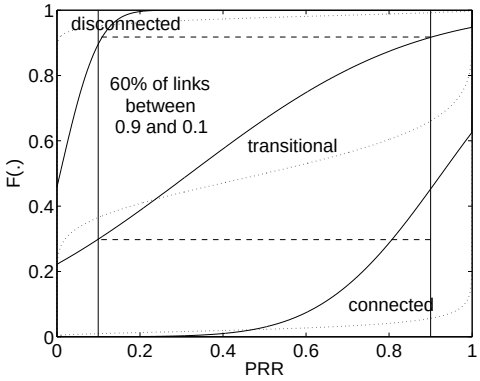

Fig. 7. Comparison of *cdf*s between the Gaussian model (black curves) and our analytical model (dotted curves) for receivers in different regions.

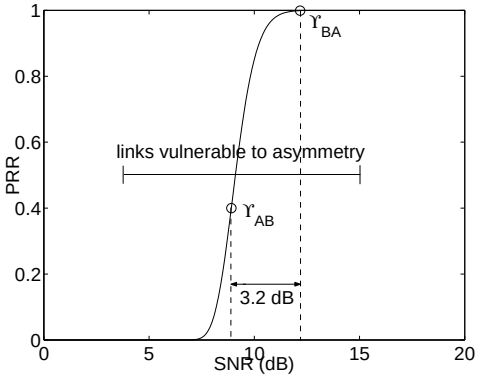

Fig. 8. Impact of hardware variance on asymmetric links.

larger the error because the width of the receiver threshold starts to be comparable with the width of the bell of the Gaussian curve which leads to a less accurate linearization. However, for common values of σ [10] the bell is significantly wider than the receiver threshold and the approximation errors are not significant. Also, while the expectation decreases monotonically with distance, the variance has a bell shape whose maximum lies in the transitional region; this behavior agrees with empirical observations in [3].

D. Comparison With Available Link Models

Some popular wireless network simulators [17], [18] and recent studies [3] had been using a Gaussian random variable to represent the packet reception rate. The PRR function based on the Gaussian model (Ψ_G) has the following form:

$$\Psi_G = \begin{cases} 1, & X > 1 \\ x, & 0 \leq X \leq 1 \\ 0, & X < 0 \end{cases} \tag{21}$$

Where X is a Gaussian random variable with parameters $\mu = E[\Psi]$ and $\sigma^2 = Var(\Psi)$. The Gaussian model leads to the following *cdf* F_G:

$$F_G(\psi) = \begin{cases} 1 - Q(\frac{-E[\Psi]}{\sqrt{V[\Psi]}}), & \psi = 0 \\ 1 - Q(\frac{\psi - E[\Psi]}{\sqrt{V[\Psi]}}), & 0 < \psi < 1 \\ 1, & \psi = 1 \end{cases} \tag{22}$$

Figure 7 shows a comparison between the *cdf*s of the Gaussian model (equation 22) and our analytical model (equation 10) for receivers in the connected, transitional and disconnected regions. Contrary to the analytical *cdf*, where links have higher probability of being either good or bad (above 0.9 or below 0.1 PRR), the Gaussian model leads to links that have a high probability of being between 0.9 and 0.1; 60% for the transitional region and 40% for the connected region, which may lead to misleading results in protocol testing. The results shown are for $\eta = 3$, $\sigma = 3$ and a non-coherent FSK radio, but similar trends are obtained for different parameters.

IV. Impact of Hardware Variance

In the previous section it was assumed that all radios have the same output power P_t and noise floor P_n, however, hardware variance induces some fluctuation around the output power set by the user and around the average noise floor. This variance problem is partially solved during the manufacturing process, where radios with a low output power and/or a high noise floor (low sensitivity) are usually discarded. However, no upper-bound is used in the filtering process and hardware variance remains as a problem. As stated in [20]: *This filtering process is justifiable, since radios that are more powerful or more sensitive are generally desirable*.

Hardware variance has already been identified as the cause of asymmetric links [1]. In this section, we not only quantify the effect of hardware variance on link asymmetry, but we also show that hardware variance can have a significant impact on the extent of the transitional region.

It is important to notice that while the output power variance can be calibrated to the same value for all radios, the noise floor variance can not be eliminated through calibration since it depends on the thermal noise generated by the underlying solid state structure.

A. Model

Hardware variance causes Gaussian distributions (in dB) in the output power and noise floor [20]. In order to capture these effects let us redefine equation 3 by denoting SNR_{AB} as the signal-to-noise ratio measured at B for the output power of A, then SNR_{AB} (Υ_{AB}) is given by:

$$\begin{aligned} \Upsilon_{AB} &= P_{tA} - PL(d) - P_{nB} \\ &= \mathcal{N}(P_t, \sigma_{tx}) - PL(d) - \mathcal{N}(P_n, \sigma_{rx}) \end{aligned} \tag{23}$$

Where σ^2_{tx} are σ^2_{rx} are the variances of the output power and the noise floor respectively, and $PL(d) = PL(d_0) + 10\ \eta\ log_{10}(\frac{d}{d_0}) + \mathcal{N}(0, \sigma)$ is the channel path loss (which is identical in both directions: $A \rightarrow B$ and $B \rightarrow A$).

Empirical measurements (Section V) show that there is some correlation between the output power and noise floor within the same radio. Our model captures this correlation by representing the output power and noise floor as a multivariate Gaussian distribution, as shown below:

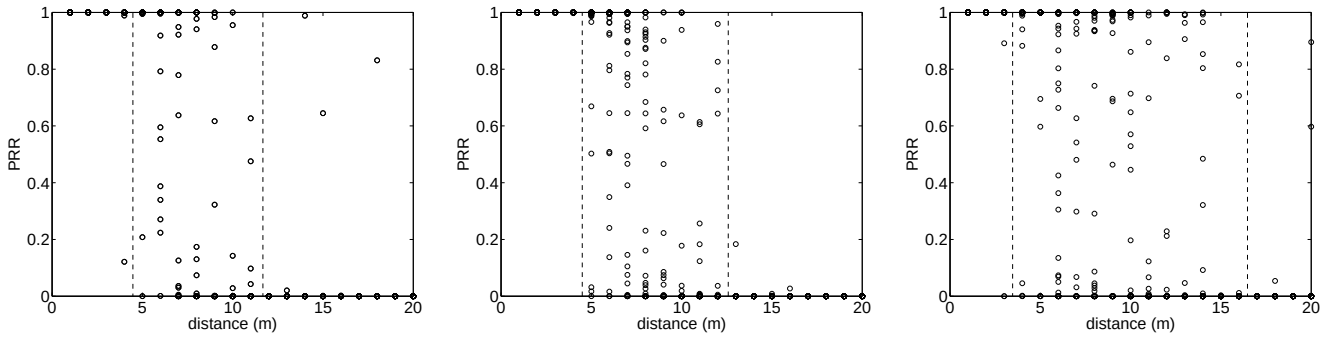

Fig. 9. Impact of channel and radio dynamics on extent of transitional region, (a) Impact of channel dynamics (real channel + identical non-variant hardware), (b) Impact of hardware variance (ideal channel + hardware variance), (d) Combined impact of channel and radio dynamics.

$$\begin{pmatrix} T \\ R \end{pmatrix} \sim \mathcal{N}\left(\begin{pmatrix} P_t \\ P_n \end{pmatrix}, \begin{pmatrix} S_T & S_{TR} \\ S_{RT} & S_R \end{pmatrix}\right) \tag{24}$$

Where P_t is the nominal output power, P_n is the average noise floor, S the covariance matrix between the output power and noise floor; and T and R are the actual output power and noise floor of a specific radio, respectively.

B. Impact on Asymmetric Links

When the output power level of all the nodes is set to the same value, radios with identical non-variant hardware (σ_{tx} = 0, σ_{rx} = 0) lead to the same SNR in both directions ($\Upsilon_{AB} = \Upsilon_{BA}$ according to equation 23), which in turn leads to the same packet reception rate (symmetric links).

For radios with hardware variance, Υ_{AB} can be different from Υ_{BA}. Figure 8 shows the effect of $\Upsilon_{AB} - \Upsilon_{BA}$ on link asymmetry. Due to the sharp threshold of the receiver, a small value of $\Upsilon_{AB} - \Upsilon_{BA}$ ($\sim$ 3.2 dB) may lead to significantly different packet reception rates in both directions (1.0 and 0.4).

$\Upsilon_{AB} - \Upsilon_{BA}$ is a random variable and the larger the variance of this difference, the higher the probability of link asymmetry. In order to quantify the impact of hardware variance on link asymmetry we will analyze the variance of $(\Upsilon_{AB} - \Upsilon_{BA})$.

Letting (T_A, R_A) and (T_B, R_B) be the respective output power and noise floor of radios A and B, then:

$$\begin{aligned} \Upsilon_{AB} - \Upsilon_{BA} &= (T_A - PL(d) - R_B) - \\ &\quad (T_B - PL(d) - R_A) \\ &= (T_A + R_A) - (T_B + R_B) \end{aligned} \tag{25}$$

$(T_A + R_A)$ and $(T_B + R_B)$ are gaussian random variables representing the sum of the output power and noise floor of *different* radios (A and B), and can be assumed to be independent[9]. $(T_A + R_A)$ and $(T_B + R_B)$ are generated from the same multivariate Gaussian distribution and can be represented by $(T + R)$, hence, $Var(\Upsilon_{AB} - \Upsilon_{BA}) = 2 \times Var(T + R)$[10], and:

$$\begin{aligned} Var(T+R) &= E[(T+R)^2] - E^2[T+R] \\ &= E[T^2] - E^2[T] + E[R^2] - E^2[R] \\ &\quad + 2(E[TR] - E[T]E[R]) \\ &= Var(T) + Var(R) + 2Cov(T,R) \\ &= S_T + S_R + 2S_{TR} \end{aligned} \tag{26}$$

Which leads to:

$$Var(\Upsilon_{AB} - \Upsilon_{BA}) = 2(S_T + S_R + 2S_{TR}) \tag{27}$$

Where S_T, S_R and S_{TR} are elements of the covariance matrix in equation 24.

Equation 27 shows that a positive correlation (positive S_{TR}) between the output power and noise floor of a radio leads to a high variance of $\Upsilon_{AB} - \Upsilon_{BA}$ (higher probability of link asymmetry), while a negative correlation (negative S_{TR}) reduces the variance (lower probability of link asymmetry). Hence, a negative correlation between the output power and noise floor leads to the lowest probability of link asymmetry, followed by zero correlation and positive correlation. Notice that a negative correlation implies that nodes with output powers higher than P_t (better transmitter) will usually have a noise floor lower than P_n (better receiver), and *vice versa*.

C. Impact on Extent of Transitional Region

In equation 3, the randomness of the SNR was due uniquely to multi-path effects, but the variance of the output power and noise floor introduces two other sources of randomness. The combined effect of output power variance, channel multi-path and noise floor variance led to a new expression for the SNR (equation 23). Based on this equation the SNR Υ is given by:

$$\begin{aligned} \Upsilon &= \mathcal{N}(P_t, \sigma_{tx}) - PL(d) - \mathcal{N}(P_n, \sigma_{rx}) \\ &= \mathcal{N}(P_t - P_n, \sigma_{hw}) - PL(d) \end{aligned} \tag{28}$$

[9]The manufacturing process can create some correlation among different radios if different batches are produced from special high (low) quality materials, but we assume that all radios belong to the same process.

[10]This is derived from the facts that for a random variable X, $Var(X) = Var(-X)$; and for $i.i.d$ random variables X_i, $Var(\sum_i X_i) = \sum_i Var(X_i)$.

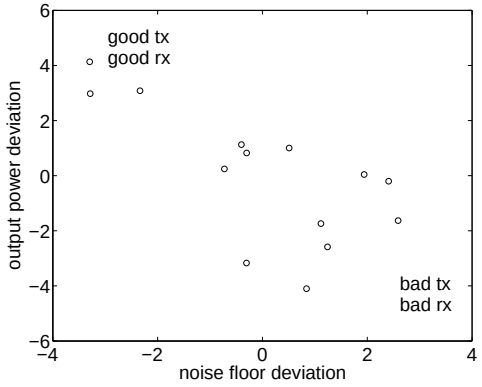

Fig. 10. Correlation between output power and noise floor.

Where $\sigma_{hw}^2 = \sigma_{tx}^2 + \sigma_{rx}^2$. Finally, Υ is given by:

$$\begin{aligned} \Upsilon &= \mathcal{N}(P_t - P_n, \sigma_{hw}) - \overline{PL(d_0)} + \mathcal{N}(0, \sigma_{ch}) \\ &= \mathcal{N}(P_t - \overline{PL(d_0)} - P_n, \sigma_t) \end{aligned} \tag{29}$$

Where $\overline{PL(d_0)} = PL(d_0) + 10\ \eta\ log_{10}(\frac{d}{d_0})$, and the total variance of the system (σ_t) is given by:

$$\begin{aligned} \sigma_t^2 &= \sigma_{ch}^2 + \sigma_{tx}^2 + \sigma_{rx}^2 \\ &= \sigma_{ch}^2 + \sigma_{hw}^2 \end{aligned} \tag{30}$$

The hardware variance generates a pseudo-path loss variance (σ_{hw}). Equation 9 showed that the larger the variance, the larger the extent of the transitional region; hence, radios with hardware variance will always increase the extent of the transitional region.

To obtain accurate results for the extent of the transitional region, σ should be replaced by σ_t in all corresponding equations in Section III. The impact of hardware variance on the extent of the transitional region can be observed in Figure 9, which presents simulated link qualities for $\eta = 3$, $\sigma_{ch} = 3$ and $\sigma_{hw} = 3$. Figure 9 (a) shows the transitional region when invariant hardware is placed in a real channel (effect of σ_{ch}^2), Figure 9 (b) presents a hypothetical scenario where variant hardware is placed in an ideal scenario (no multi-path effects), we observe that even in the absence of multi-path effects a transitional region is observed due to the pseudo-variance σ_{hw}^2. Finally, Figure 9 (c) presents the combined effects of σ_{ch} and σ_{hw}, showing a larger transitional region than in Figures 9 (a) and (b).

V. Empirical Validation

We now present empirical results conducted in static and low-dynamic environments to validate our analytical results on the impact of η, σ_{ch} and σ_{hw} on the extent of the transitional region. We will also observe that the correlation between output power and noise floor in mica2 motes is negative, which is the least damaging in terms of link asymmetry among the different correlations (positive, zero, negative).

We considered two environments, an indoor environment (aisle of a building), and an outdoor environment (football field). All the measurements were made using mica2 motes.

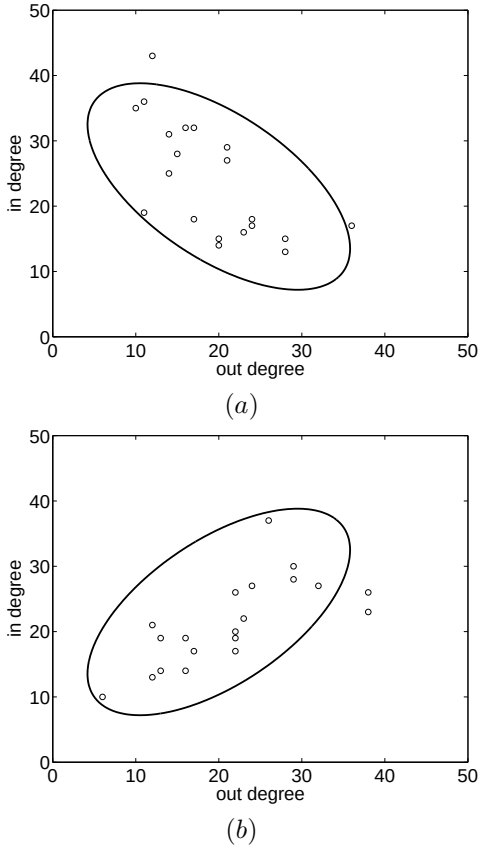

Fig. 11. Simulation results for the relation between in-degree and out-degree, (a) positive correlation, (b) negative correlation.

These devices use Non-Coherent FSK modulation at 915 MHz with Manchester encoding and provide data rates of 38.4 Kbaud.

A. Channel and Radio Parameters

Channel: Two motes were used to measure the path loss exponent (η), the variance (σ_{ch}^2) and the initial decay $PL(d_0)$ of the channel. Table III presents the values for η and σ_{ch}. The reference distance (d_0) of the log-normal model was set to 1m and its corresponding power decay was found to be 55 dB.

Radio: One mote was selected as a common receiver and sender to capture the variance of the output power P_t and noise floor P_n. The measurements were done in a isolated empty room, where each mote had the same source power and was placed at the same physical position with respect to the reference mote. Figure 10 presents the empirical measurements, which shows a negative correlation between output power and noise floor. From our experiments, the resultant covariance matrix is given by:

environment	η (95% conf. bounds)	σ_{ch} (95% conf. bounds)
outdoor	4.7 (4.3 - 5.1)	3.2 (2.6 - 3.8)
indoor	3.3 (2.1 - 4.5)	5.5 (4.6 - 6.8)

TABLE III
Channel Parameters

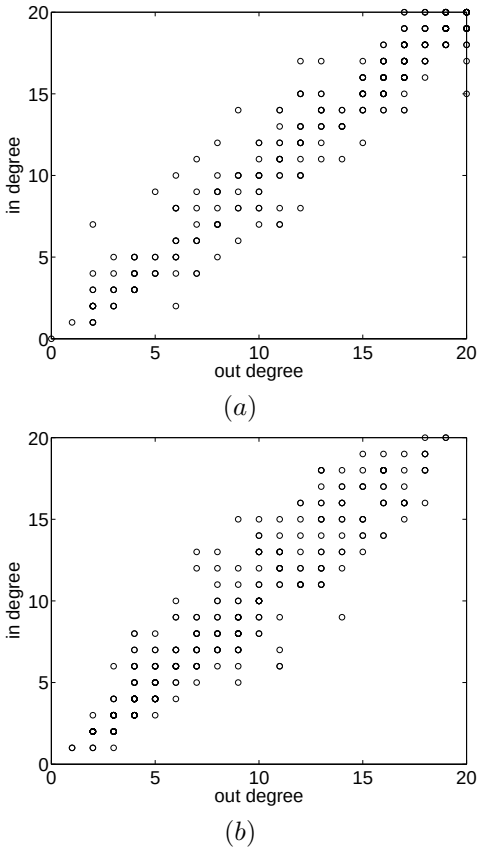

Fig. 12. Empirical correlation between in-degree and out-degree for different power levels, (a) indoor environment, (b) outdoor environment.

$$\mathrm{S} = \begin{pmatrix} 6.0 & -3.3 \\ -3.3 & 3.7 \end{pmatrix}$$

The standard deviations of the output power (σ_{tx}) and noise floor (σ_{rx}) are presented in table IV, these values lead to $\sigma_{hw} = 3.0$. Different power levels were tested and all levels showed a similar variance.

The negative correlation of mica2 motes is due to several factors. Nowadays chip implementation is moving toward single chip design, and hence, the performance of the transmitter and receiver is determined by the common underlying solid-state structure. Board implementation and antenna gains further enhance this correlation since a common path goes from the antenna to the chip. Hence, a radio with a good solid-state structure (low thermal noise) and a high path-antenna gain will lead to higher output powers (good transmitter), and a lower noise floor (good receiver). Also, while our measurements where done in controlled scenarios, characteristics of real deployments such as the remaining output power of batteries, may further enhance the correlation.

It is important to observe that this negative correlation leads to some nodes being good transmitters and receivers which may create some cluster behavior, as observed in some empirical studies [1], [8].

The negative correlation has a direct impact on the relation

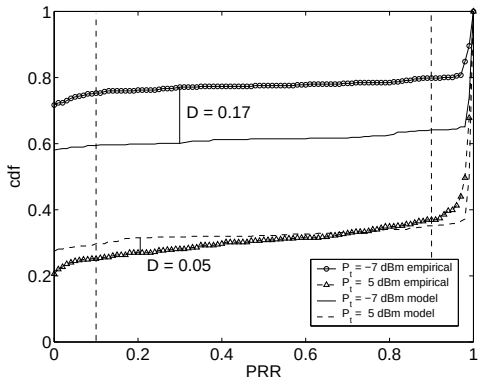

Fig. 13. Kolmogorov-Smirnov test between the empirical and model-generated packet reception rate for medium and high output powers in a grass area.

between the out-degree and in-degree of nodes[11]. In section IV-B we had stated that the negative correlation between the output power and noise floor leads to the lowest level of link asymmetry which implies that the in-degree and out-degree of nodes will be more similar than for positive and zero correlations. Figure 11 shows simulation results for the relation between in-degree and out-degree for positive and negative correlations between the output power and noise floor. It can be observed the close relation between in-degree and out-degree for the negative correlation. Figure 12 shows the empirical in-degree/out-degree relation of all nodes for all the tested power levels[12], and we can observe that the empirical trend agrees with the simulation results. This close relation between in-degree and out-degree is highly desirable given the strong dependance that several medium access and network layer protocols have on symmetric links. Hence, from all types of hardware variances a negative correlation between output power and noise floor is the least damaging in terms of link asymmetry.

Noise Floor: Given that our work does not consider interference, the noise floor can be obtained by the well-known thermal noise equation [23], which leads to a value of

[11]In-degree is the number of neighbors that can communicate with a specific node, out-degree is the number of neighbors that a specific node can communicate with.

[12]Links were considered valid if they had a PRR above 10%. The same trend is observed for any blacklisting threshold.

		(95% conf. bounds)
output power	σ_{tx}	2.3 (1.7 - 3.5)
noise floor	σ_{rx}	1.9 (1.4 - 3.1)

TABLE IV
RADIO PARAMETERS

	Expected σ_t	Measured σ_t	Measured σ_{ch}
indoor	6.3	6.1	5.5
outdoor	4.8	5.1	3.2

TABLE V
COMPARISON OF σ_t

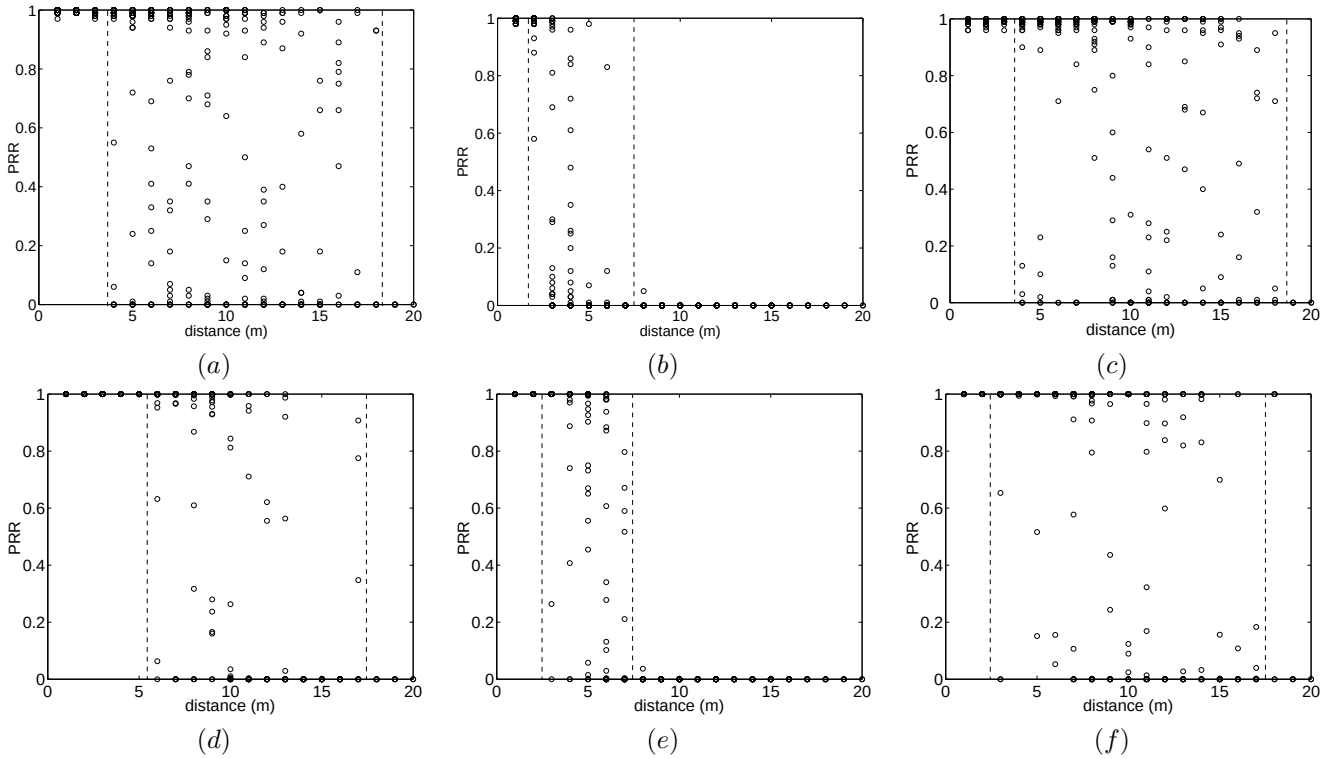

Fig. 14. Comparison of empirical measurements and instances of analytical model, (a) Empirical indoor P_t=-7dB, (b) Empirical outdoor P_t=-7dB, (c) Empirical outdoor P_t=5dB, (d), (e) and (f) are the analytical counterparts.

-115 dBm for the parameters of the radio chip [24]. However, our measurements showed that the average noise floor is approximately -105 dBm, the 10 dB difference is mainly due to losses from the output-pin of the chip to the antenna, which are not considered in the thermal noise equation. These losses depend on board implementation and are beyond the scope of this work. Hence, for the model, the average noise floor P_n will be set to -105 dBm.

Finally, it is important to consider that bit-error-rate expressions are usually given in terms of $\frac{E_b}{N_0}$ (known as SNR per bit), however, most commercially available radios provide only RSSI measurements, which can be converted to SNR per packet (Υ). Υ has a simple relation with $\frac{E_b}{N_0}$: $\Upsilon = \frac{E_b}{N_0}\frac{R}{B_N}$, for mica2 motes R = 19.2 kbps (data rate) and B_N = 30 kHz (noise bandwidth). Hence, all RSSI measurements can be converted to $\frac{E_b}{N_0}$ values.

B. Chain Topologies

For each environment, a chain topology of 21 motes was deployed with nodes spaced 1 meter apart. The frame size was 50 bytes with a preamble of 28 bytes. A simple TDMA protocol was implemented to avoid collisions. Every mote transmitted 100 packets at a rate of 5 packets/sec. Upon reception of a packet the sequence number and the received signal strength (P_r) were stored; simultaneously, the noise floor was sampled. The average SNR and packet reception rate were measured for all the links in the network.

	beginning (m)	end (m)
indoor P_t= -7dB	4.8	23.4
outdoor P_t= -7dB	3.4	8.1
outdoor P_t= 5dB	6.1	14.6

TABLE VI
ANALYTICAL EXTENT OF TRANSITIONAL REGION

According to equation 30, the expected total variance is the sum of the channel and radio variances (sum of variances of tables III and IV). Table V shows the expected σ_t, the measured σ_t and the σ_{ch}. The expected σ_t is derived from the σ_{ch} and σ_{hw} of tables III and IV, and the measured σ_t is obtained from the chain topology experiment. We observe that the expected and measured σ_t are similar. It can also be observed that σ_{ch} is smaller than σ_t (specially for the outdoor environment) confirming that hardware variance contributes to the total variance, and consequently to the extent of the transitional region.

In order to validate our model we present two comparisons. The first one is a formal method based on the Kolmogorov-Smirnov (K-S) test and the second one is a comparison of the packet reception rates versus distance between empirical and simulated data. Figure 13 presents the cumulative distribution of the packet reception rate for the chain topology described above. Two power levels, -7 dBm and 5 dBm, are presented for the outdoor environment. For the number of links in the chain topology (420) and a confidence interval of 10% the K-S table has a threshold value of 0.06. For practical purposes let us define links with PRR above 0.9 as reliable and neglect

STEP 0 : Radio	Obtain output power (T) and noise floor (R) for all nodes Can use Cholesky decomposition to generate multivariate r.v. equation 24 For mica2: $-20\ dBm < P_t < 5\ dBm$, $P_n = -105dBm$
STEP 1 : Channel	Obtain channel parameters $PL(d_0), n, \sigma$ Can be obtained through own empirical measurements, or from some published results [10]
STEP 2 : SNR	Obtain SNR in dB (γ_{dB}) as a function of distance d $\gamma_{dB}(d) = T - PL(d_0) - 10nlog_{10}(\frac{d}{d_0}) - N(0,\sigma) - R$
STEP 3 : Modulation	Select modulation and insert $\gamma(d)$ from previous step, but not in dB (i.e. $\gamma = 10^{\frac{\gamma_{dB}}{10}}$) Convert from $\frac{E_b}{N_0}$ to $RSSI$ by inserting appropriate bit data rate R and noise bandwidth B_N According to modulation select appropriate BER (P_e) ASK noncoherent: $\frac{1}{2}[\exp^{-\frac{\gamma(d)}{2}\frac{B_N}{R}} + Q(\sqrt{\gamma(d)\frac{B_N}{R}})]$ ASK coherent: $Q(\sqrt{\frac{\gamma(d)}{2}\frac{B_N}{R}})$ FSK noncoherent: $\frac{1}{2}\exp^{-\frac{\gamma(d)}{2}\frac{B_N}{R}}$ FSK coherent: $Q(\sqrt{\gamma(d)\frac{B_N}{R}})$ PSK binary: $Q(\sqrt{2\gamma(d)\frac{B_N}{R}})$ PSK differential: $\frac{1}{2}\exp^{-\gamma(d)\frac{B_N}{R}}$
STEP 4 : Encoding	Select packet reception rate Select according to encoding scheme, then insert frame, preamble length and P_e obtained in previous step NRZ : $(1-P_e)^{8\ell}(1-P_e)^{8(f-\ell)}$ 4B5B : $(1-P_e)^{8\ell}(1-P_e)^{8(f-\ell)1.25}$ Manchester : $(1-P_e)^{8\ell}(1-P_e)^{8(f-\ell)2.0}$ SECDED : $(1-P_e)^{8\ell}((1-P_e)^8 + 8P_e(1-P_e)^7)^{(f-\ell)3.0}$

TABLE VII
THEORETICAL MODELS FOR THE LINK LAYER

links with PRR below 0.1[13], then the distance D of the K-S test is considered between 0.1 and 0.9. We observe that low density networks such as the medium power case would not pass the test ($0.17 > 0.06$), but high density networks such as the high power case pass the test ($0.05 < 0.06$) and hence both distributions can be considered similar (empirical and simulated). It is also important to notice that the empirical data shows that most of the probability mass is either above 0.9 or below 0.1 for any output power as it was shown in Section III-D. The next comparisons will illustrate why low-dense networks are predicted less accurately than high dense networks.

Figure 14 shows the empirical packet reception rates versus distance compared to their analytical counterparts. It can be observed that the model provides a reasonable approximation of the real behavior. Table VI shows the expected beginning and end of the transitional region according to equation 8 for the scenarios in Figure 14. We can observe that this equation provides reasonable predictions for the empirical observations. Several power levels were tested, from -20 dBm to 5 dBm in steps of 1 dBm, and all power levels showed a similar behavior to the proposed model. A comparison of Figures 14 (b) and (e) provides a better understanding of why the K-S test fails to asses both distributions as similar. In the simulated case (Figure 14 (e)), the model tends to classify more links as good links than the empirical data. For instance, the simulated data shows that all links under a distance of 2 meters are considered to be 1.0, while the empirical data shows some unreliable links at a distance of 2 meters. Also, for distances 5 and 6 some links are good (> 0.9) in the simulated data, while in the empirical data most of them are below 0.9. Since the transitional region is narrow, the disagreement on a few links leads to approximately 15% of the mass probability shifting from bad links to good links, which causes the failure of the K-S test. Nevertheless, it is also worth considering that the major disagreement is only on the differences at the extremes (good and bad links), the slope for the unreliable links is similar, showing that both empirical and modeled data have a close approximation on the number of unreliable links. It is important to mention that our model is not meant to be a exact replica of the environment but an approximation to it.

[13]A very reasonable assumption considering that links below 0.1 would incur in significant losses or in high number of retransmissions

VI. CONCLUSION

The impact that channel and radio dynamics have on the performance of upper-layer protocols in wireless sensor networks requires a clear understanding of the behavior of the wireless link. The analysis presented allowed us to quantify the impact of channel multi-path and hardware variance on unreliable and asymmetric links. The main contributions of this work are:

- A systematic approach to obtain mathematical link layer models for the statistical variation of packet reception rates with respect to distance was presented. Model generators can be downloaded from:
  http://ceng.usc.edu/∼anrg/downloads.html

- Analytical expressions for the boundaries of the transitional region were derived.

The advantage of our model is that the communication theory literature has channel parameters for different environments, and even though every environment is unique these parameters can be used to obtain a first approximation of the link behavior. If channel measurements are already available for the type of environment where the motes will be deployed, then there is no need to deploy the motes in-situ to obtain the behavior of the link. The characteristics of the radio can be determined independently –receiver response (PRR vs SNR) and hardware variance– and when combined with the channel measurements will give an approximation of the link behavior. In cases where there are no prior measurements of the channel, all the previous proposed models (including ours) requires in-situ measurements.

The key conclusions of our study are:

- The relative size of the transitional region (Γ coefficient) is higher for lower path loss exponents and higher variances.
- Hardware variance induces a pseudo-variance, which increases the size of the transitional region.
- A negative correlation between the output power and noise floor leads to lower levels of asymmetry, which is highly desirable given the number of protocols that heavily depend on symmetric links.
- The negative correlation also leads to nodes that are good transmitters and receivers, which helps to explain the clustering behavior observed in previous works [1], [8].
- Even with a perfect-threshold radio, the transitional region still exists as long as there are multi-path effects.

Even though the simulations and empirical validation were based on radios using NC-FSK modulation and Manchester encoding, the model can be easily extended to other radio characteristics. Table VII presents the steps required for other common modulation techniques and encoding schemes.

It is important to highlight that while different modulations, encoding and packet sizes lead to different sizes of the regions, they do not significantly affect the Γ coefficient, and hence, the results were not presented in the interest of space. Some of the results are presented in [14].

Our work contributes to a better understanding of the behavior of low-power wireless links but is not exhaustive. It can be complemented with other studies to capture other important phenomenon present in real scenarios; for instance, contention models from [13], temporal properties from [19] and correlations due to direction of propagation from [7] (Appendix I).

It is important to recall that physical layer dynamics, appearing as the transitional region at the link layer, are not only potential causes of a negative impact, but they can have a positive impact as well. For example, [22], [21] report that multi-path effects have a positive impact on the connectivity of random topologies, and in [16], an early version of the model presented in this paper ([14]) was used to obtain optimal forwarding distances for geographic routing. Hence, given the requirements of the application, our work provides a tool to the network designer to improve the overall performance of the protocols.

Finally, from preliminary results (Appendix II), we find that even spread spectrum radios show transitional region effects; we therefore believe there is value in extending this work to other settings.

ACKNOWLEDGMENT

The authors would like to acknowledge assistance from and useful conversations with Prof. Urbashi Mitra, Dr. Alec Woo, Dr. Jerry Zhao, Prof. John Heidemann, Dr. Robert Poor, and Prof. Scott Shenker.

REFERENCES

[1] D. Ganesan, B. Krishnamachari, A. Woo, D. Culler, D. Estrin and S. Wicker, *"Complex Behavior at Scale: An Experimental Study of Low-Power Wireless Sensor Networks"*, UCLA CS Technical Report UCLA/CSD-TR 02-0013, 2002.

[2] J. Zhao and R. Govindan, *"Understanding Packet Delivery Performance in Dense Wireless Sensor Networks"*, ACM Sensys '03, Los Angeles, California.

[3] A. Woo, T. Tong, and D. Culler, *"Taming the Underlying Issues for Reliable Multhop Routing in Sensor Networks"*, ACM Sensys '03, Los Angeles, California.

[4] A. Cerpa, N. Busek, and D. Estrin, *"SCALE: A tool for Simple Connectivity Assessment in Lossy Environments"*, CENS Technical Report, September 2003.

[5] D. S. J. De Couto, D. Aguayo, J. Bicket, and R. Morris, *"A High-Throughput Path Metric for Multi-Hop Wireless Routing"*, ACM MobiCom '03, San Diego, California.

[6] D. Kotz, C. Newport and C. Elliott, *"The mistaken axioms of wireless-network research"*, Technical Report TR2003-467, Dept. of Computer Science, Dartmouth College, July 2003.

[7] G. Zhou, T. He, S. Krishnamurthy, and J. Stankovic, *"Models and solutions for radio irregularity in wireless sensor networks"*, ACM Transactions on Sensor Networks (TOSN), Volume 2, Issue 2, May 2006.

[8] A. Cerpa, J. L. Wong, L. Kuang, M. Potkonjak and D. Estrin, *"Statistical Model of Lossy Links in Wireless Sensor Networks"*, IEEE/ACM IPSN'05, Los Angeles, California.

[9] D. Lal, A. Manjeshwar, F. Herrmann, E. Uysal-Biyikoglu, A. Keshavarzian, *"Measurement and Characterization of Link Quality Metrics in Energy Constrained Wireless Sensor Networks"*, IEEE Globecom '03, San Francisco, California.

[10] K. Sohrabi, B. Manriquez, and G. Pottie, *"Near Ground Wideband Channel Measurement"*, IEEE Vehicular Technology Conference, 1999.

[11] S. Y. Seidel and T. S. Rapport, *"914 MHz Path Loss Prediction Model for Indoor Wireless Communication in Multi floored Buildings"*, In IEEE Transactions on Antennas and Propagation, volume 40(2), pages 207-217, February 1992.

[12] H. Nikookar and H. Hashemi, *"Statistical modeling of signal amplitude fading of indoor radio propagation channels"*, 2nd International Conference on Universal Personal Communications, 1993.

[13] D. Son, B. Krishnamachari and J. Heidemann, *"Experimental Analysis of Concurrent Packet Transmissions in Low-Power Wireless Networks"*, ACM SenSys '06, Boulder, Colorado.

[14] M. Zuniga and B. Krishnamachari, *"Analyzing the Transitional Region in Low Power Wireless Links"*, IEEE SECON '04, Santa Clara, California.

[15] D. Son, B. Krishnamachari, and J. Heidemann. Experimental study of the effects of Transmission Power Control and Blacklisting in Wireless Sensor Networks. IEEE SECON '04, Santa Clara, California.

[16] K. Seada, M. Zuniga, A. Helmy and B. Krishnamachari, *"Energy Efficient Forwarding Strategies for Geographic Routing in Wireless Sensor Networks"*, ACM Sensys 2004, Baltimore, Maryland.

[17] P. Levis, N. Lee, M. Welsh, and D. Culler, *"TOSSIM: Accurate and scalable simulation of entire tinyos applications"*, ACM Sensys '03, Los Angeles, California.

[18] L. Girod, J. Elson, A. Cerpa, T. Stathopoulos, N. Ramanathan, D. Estrin, *"EmStar: a Software Environment for Developing and Deploying Wireless Sensor Networks"*, USENIX '04, Boston, Massachusetts.

[19] A. Cerpa, J. L. Wong, M. Potkonjak and D. Estrin, *"Temporal Properties of Low Power Wireless Links: Modeling and Implications on Multi-Hop Routing"*, ACM Mobihoc '05, Urbana-Champaign, Illinois.

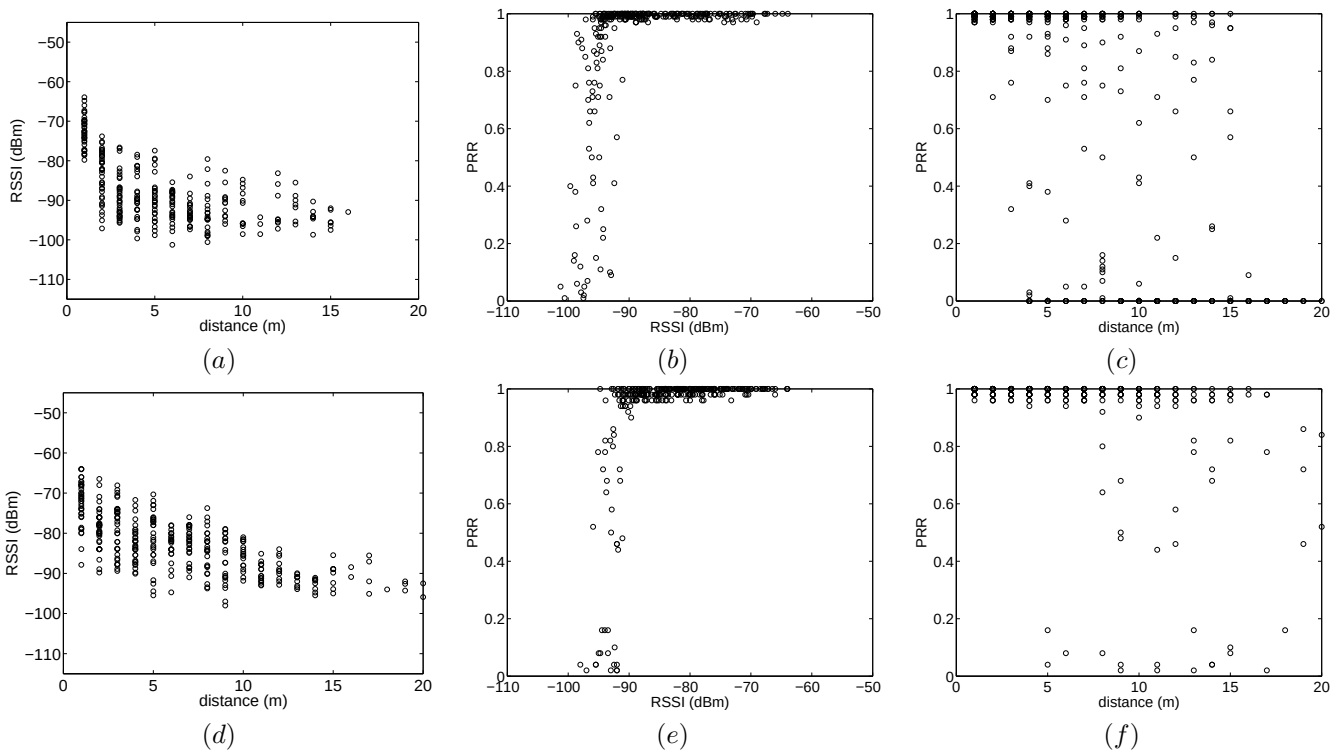

Fig. 15. Comparison of empirical measurements for channel, radio and link between mica2 and micaZ motes, P_t = -10 dBm for both type of motes, (a) channel mica2, (b) radio mica2, (c) link mica2, (d), (e), (f) are their micaZ counterparts.

[20] R. Poor, *"Sources of Asymmetry in Wireless Mesh Sensor Networks"*, private communication, 2004.

[21] C. Bettstetter and C. Hartmann, *"Connectivity of Wireless Multihop Networks in a Shadow Fading Environment"*. ACM MSWiM '03, San Diego, California.

[22] E. Altman and D. Miorandi, *"Coverage and connectivity of ad-hoc networks in presence of channel randomness"*, IEEE INFOCOM '05, Miami, Florida.

[23] Theodore S. Rappapport *"Wireless Communications: Principles and Practice"*, Prentice Hall.

[24] Chipcon. CC1000 low power radio transceiver, "http://www.chipcon.com/files/CC1000_Data_Sheet_2_2.pdf".

APPENDIX I

In [7] the authors present the degree of irregularity (DOI) coefficient as a means to capture the variation per unit degree change in the direction of radio propagation. In that work the received power is given by:

$$\begin{aligned} P_r(d) &= P_t \ - \ DOIAdjustedPathLoss \ + \ \mathcal{N}(0,\sigma) \\ &= P_t \ - \ PathLoss \times K_i \ + \ \mathcal{N}(0,\sigma) \end{aligned} \tag{31}$$

Where K_i is a coefficient to represent the difference in path loss in different directions. The method to obtain this coefficient is presented in the RIM model [7].

Denoting $10\eta log_{10}(\frac{d}{d_0})$ by $\overline{PL(d_0)}$, equation 1 can be modified to include non-isotropic effects:

$$P_r(d) = P_t \ - \ \overline{PL(d_0)} \times K_i \ + \ \mathcal{N}(0,\sigma) \tag{32}$$

The effect of obstacles can be included by inserting a new variable on the previous equation. Let us denote Ω_{vw} as the path loss in dB due to an obstacle – for example a wall – between nodes v and w. Then, letting v be the transmitter, the received power at w is given by:

$$P_{r_w}(d) = P_{t_v} \ - \ (\overline{PL(d_0)} + \Omega_{vw}) \times K_i \ + \ \mathcal{N}(0,\sigma) \tag{33}$$

Hence, if the layout of the environment is provided, the above equation can be used to include additional path loss for each pair of nodes according to the obstacles between them.

APPENDIX II

Some preliminary empirical evaluations were done with micaZ devices. These motes have a 2.4 GHz IEEE 802.15.4/ZigBee(tm) RF transceiver, which uses DSSS modem with 2 Mchips/s and 250 kbps effective data rate. A chain topology with the same methodology as in subsection V-B was deployed in the same indoor environment as mica2 motes.

Figure 15 compares empirical measurements for the channel, radio, and links for mica2 and micaZ motes. The nominal output power for both types of motes was -10 dBm. We observe that the transitional region still has a significant extent. However, for the same output power micaZ radios seem to have a larger connected and transitional regions.

No major differences were found in the standard deviation for both deployments (around 6.1 for both). However, the path loss exponent for micaZ measurements is 1.94 which is smaller than the corresponding value for mica2 in Table III (η = 3.3) . According to equation 8 a smaller η increases the size of both regions, which provides some intuition as to why the extent of the regions are larger for micaZ motes for the same output power.

The spread spectrum techniques seem to partially combat multi-path by decreasing η and consequently providing a larger coverage for the same output power, however, as stated in equation 9 a lower η implies a larger transitional region which increases the number of unreliable and asymmetric links. An in-depth study of the impact of low-cost spread spectrum radios in the transitional region is part of our future work.